Ibn Al-Haitham Journal for Pure and Applied Sciences
Journal homepage: jih.uobaghdad.edu.iq
PISSN: 1609-4042, EISSN: 2521-3407
IHJPAS. 2024, 37(4)

Using Thomas-Fermi Formula of Level Density Parameter to Find New Single Particle Level Density Formula

Hadeer K. Mohammed[1,*] and Ali D. Salloum[2]
[1,2]Department of Physics, College of Sciences for Women, University of Baghdad, Baghdad, Iraq.
*Corresponding Author

Received: 2 May 2023 Accepted: 7 June 2023 Published: 20 October 2024
doi.org/10.30526/37.4.3455

Abstract

The level density is a parameter that has great importance in the theoretical nuclear calculation, and it is considered a key of many theoretical studies, therefore, the level density in pre-equilibrium reaction or what is the so-called accurate partial level density PLD has been studied. The partial level density PLD used in pre-equilibrium reactions is dependent on the parameter called single particle level density which can be calculated by two methods either using the equidistant spacing model (ESM) or non-equidistant spacing model (non-ESM) In this study, the parameter g is estimated by using the relation between the level density parameter g and a based on Ericson and Williams's formulas ($a = \frac{\pi^2}{6} g$) is substituted from the Thomas-Fermi formula and the new g was substituted one-component Ericson's formula, two-components Ericson's formula, Williams's formula, spin formula, and surface formula. The results show that the PLD estimated from one-component Ericson's formula gives the best agreement with the experimental data between 4 MeV to 5 MeV.

Keywords: Exciton model, induced nuclear reaction, level density, pre-compound nucleus, pre-equilibrium reactions.

1. Introduction

Many theoretical calculations, including reaction rates, cross-section, and astrophysics, use level density (L.D.) as a parameter. It is also important for medical physics and nuclear reaction design [1, 2]. The first use of the L.D. was made by the scientist Bethe in 1936 when he established the Fermi gas model [3, 4]. The parameter known as single article level density (g), representing the sum of the proton and neutron single-particle levels at the Fermi surface, determines the L.D. The Fermi gas model first used g, assuming it to be a non-degenerate and equidistant spacing model in its simplest picture, the non-degenerate and equidistant spacing model ESM [5]. We also used the non-equidistant spacing model, or non-ESM, to derive the parameter g, similar to the Exaction model [6]. Numerous studies exist on level density features, but we highlight those that are most relevant to our work, such as the calculation of the level density parameter for deformed nuclei (161-168Er and 204-210Bi). In this study, we employed collective enhancement, which encompasses the

© 2024 The Author(s). Published by College of Education for Pure Science (Ibn Al-Haitham), University of Baghdad. This is an open-access article distributed under the terms of the Creative Commons Attribution 4.0 International License

rotational ground state modes at neutron binding energy. We obtained these modes using both ESM and non-ESM for each isotope, and we compared them with other models and experimental data [7]. We also studied the effect of the deformation parameter on the nuclear level density parameter for certain radioisotopes (Dy, W, and Os), focusing on level density values that correspond to energies from the observed spectra near the neutron binding energy. The calculations were done in the framework of ESM, and the results have good agreement when they are compared with the s-wave neutron resonance data [8]. In this paper, a new formula for the parameter g is derived using the relation between g and the level density parameter a (a= π^2/6 g) [9]. The study aims to use the new formula g in the calculation of PLD in a pre-equilibrium region, and then compare the results with the experimental values of PLD to test the validity of the new formula.

2. Materials and Methods

Ericson's formula and several corrected formulas give the level density in the pre-equilibrium region of nuclear reactions [10]. A more accurate expression refers to the level density in the pre-equilibrium region as partial level density (PLD), as it excites some nucleons in the nucleus when protons and neutrons are considered indistinguishable particles [10].

$$\omega_1(n,E) = \frac{g^n E^{n-1}}{p!h!(n-1)!} \quad (1)$$

The symbols ω_1(n,E) are the PLD, E excitation energy, p particle number,h hole number and $n = p + h$ is the exciton number, which represents the sum of the particle number and the hole number. The parameter g is the single particle level density we will discuss it in detail later. If the protons and the neutrons are considered as distinguishable particles, the PLD is given by two-component Ericson's formula [6].

$$\omega_2(\mathrm{n,\ E}) = \frac{(g_\pi)^{n\pi}\,(g_\upsilon)^{n\upsilon} E^{n-1}}{p_\pi!h_\pi!p_\upsilon!h_\upsilon!(n-1)!} \quad (2)$$

p_π the proton particles, h_π is the proton holes, p_ν is the neutron particles, h_ν is the neutron holes, n_π is the proton exciton numbers and n_υ is the neutrons exciton number. The symbols g_π and $\mathrm{g_\upsilon}$ are single particle level densities for protons and neutrons, respectively.

Many corrections were added to the PLD formula; one of them is shown in William's formula, which contains effect 1 of Pauli's exclusion principle in William's formula [6].

$$\mathrm{w_{1(n,E)}} = \frac{\mathrm{g^n\,(E-A(p,h))^{n-1}}}{\mathrm{p!h!(n-1)!}} \quad (3)$$

$$A_{(p,h)} = \frac{p(p+1)+h(h-3)}{2g} \quad (4)$$

The second correction is the spin correction which means adding the spin effect to the PLD formula that is represented by the factor $R(J)$, then the PLD formula becomes [10].

$$W_{1(n,E)} = \frac{g^n E^{n-1}}{p!h!(n-1)!}\, R(J) \quad (5)$$

$$R(J) = \frac{2j+1}{2\sqrt{2\pi\sigma_n^3}} exp\left[-\frac{(j+\frac{1}{2})^2}{2\sigma_n^2}\right] \quad (6)$$

σ_n is the cut-off parameter, J is the total angular momentum.

The third correction is the surface correction, which is because the nuclear potential at the surface of the nucleus is shallower than it is inside the nucleus [6].

$$\omega_1(n,E,V) = \omega_1(n,E,\infty) \times f_1(n,E,V) \quad (7)$$

$$f_1(n,E,V) = \sum_{j=0}^{h}(-1)^j C_j^h \left[\frac{E-jV(h)}{E}\right]^{n-1} \Theta\,(E-jV(h)) \quad (8)$$

The parameter g can be given either in the framework of the equidistant spacing model ESM or by the non-equidistant spacing model (non-ESM) [8]. In this study, we will derive a new formula of g using the relation between the level density parameter a and g [11, 1].

$$g = \frac{6}{\pi^2} a \quad (9)$$

The parameter a from the Thomas-Fermi formula.

$$a = (0.109(1-4.476I^2)A + 0.076(1+31.47I^2)A^{2/3} - 0.0024Z^2A^{-1/3}) \quad (10)$$

I Represents isospin, Z is the atomic number, A is the mass number
Then, g become

$$g = \frac{6}{\pi^2}\,(0.068A + 0.213A^{2/3} + 0.385A^{1/3}) \quad (11)$$

In the case of two-component [6]:

$$g_\pi = \frac{Z}{A} g \quad (12)$$

$$g_\upsilon = \frac{N}{A} g \quad (13)$$

In the next section, the g formulae are substituted in all PLD formulas and compared to the results with the experimental data.

3. Results and Discussion

The discussion was made by comparing the theoretical curves that came from substituting g from the Thomas-Fermi formula in all PLD formulas mentioned above with the experimental data, and the equations are programmed using Mat. Lab.

Figure 1. shows a comparison between one-component Ericson's formula of the PLD curve with g from the Thomas-Fermi formula and the experimental data. It is noticed that the theoretical curve is less than the experimental curve up to 4 MeV and from 4 MeV to 5 MeV. Both curves become in agreement, and after 5 MeV, the theoretical curve becomes higher than the experimental curve. In other words, the theoretical curve mediates the experimental curve. In other words, the theoretical curve mediates the experimental curve. This behavior can be attributed to the g formula from Thomas-Fermi which contains A with different powers, as shown in equation (10). This makes the PLD depending on g from Thomas-Fermi increasing moderately in agreement with the experimental data.

Figure 2. shows a comparison between two components of Ericson's formula for PLD with g from the Thomas-Fermi formula and the experimental curve. Because two components divide

the energy into more particles than one, the theoretical curve lies below the experimental curve. The theoretical curve begins at 1 MeV and grows with increasing excitation energy.

Figure 3. shows a comparison between the one-component William's formula for PLD from Thomas-Fermi and the experimental data. The theoretical curve is lower than the experimental data because Pauli's principle limits the occupied energy levels. Also, it shows that the theoretical curve increases with increased excitation energy.

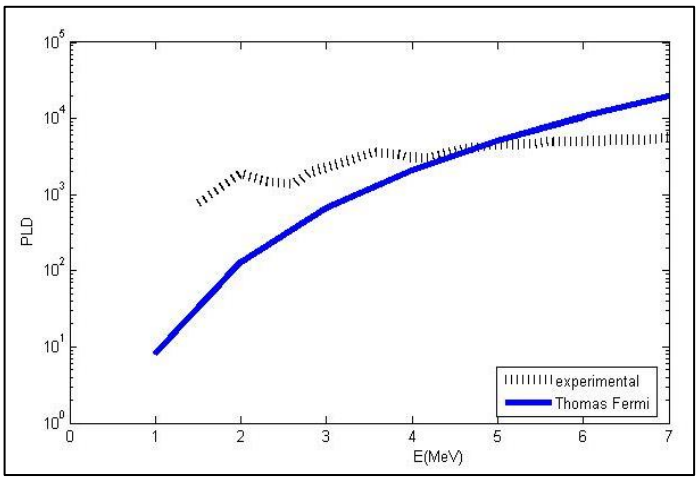

Figure 1. A comparison between the theoretical curve of PLD from one component with g from Thomas-Fermi and the experimental data.

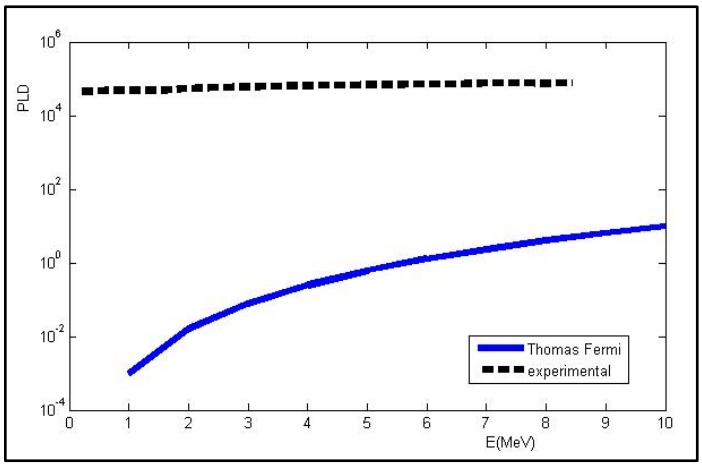

Figure 2. A comparison between the theoretical curve with g from Thomas-Fermi and the experimental data.

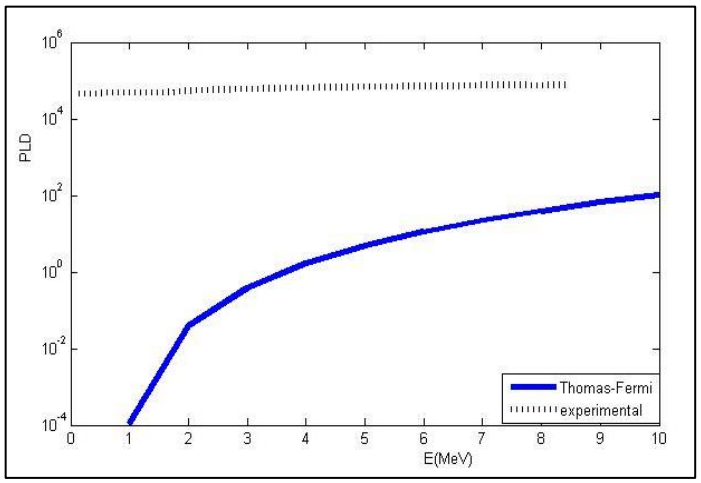

Figure 3. A comparison between the theoretical curves of PLD from Williams's with g from Thomas-Fermi and the experimental data

Figure 4. shows a comparison between the theoretical curve of PLD from spin correction with Thomas-Fermi and the experimental curve. We notice that the theoretical curve is lower than the experimental curve because the spin limits the levels occupied by particles; therefore, the level number decreases, and the PLD also decreases. The difference between them is significant at 1 MeV and decreases with increasing excitation energy.

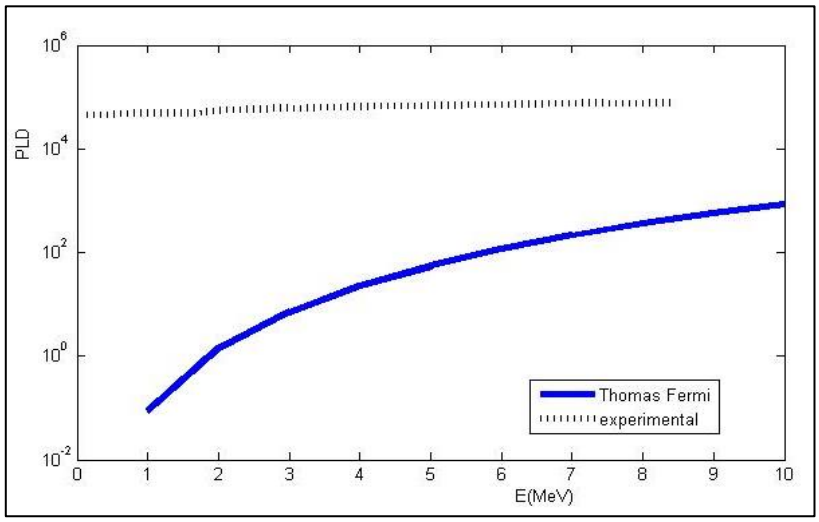

Figure 4. A comparison between the theoretical curve of PLD from spin with g from Thomas-Fermi and the experimental data.

Figure 5. gives a comparison between the theoretical curve of PLD from surface correction with Thomas-Fermi and the experimental curve. It is noticed that the theoretical curve starts at 8 MeV and increases with data, while the experimental curve starts from the origin point; therefore, the theoretical curve cannot be useful to describe the experimental data.

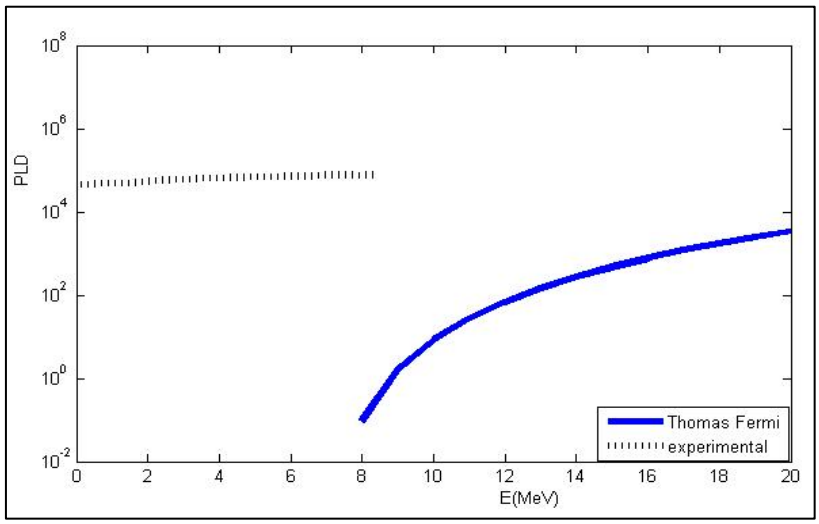

Figure 5. A comparison between the theoretical curve of PLD from the surface with g from Thomas-Fermi and the experimental data.

4. Conclusion

The theoretical curve that gives agreement with the experimental data is Ericson's curve with g from Thomas-Fermi. One can show that the curve mediates the experimental values: it starts at 1 MeV and goes up to 4 MeV; it is below the experimental curve; from 4 to 5 MeV, it agrees with the experimental data; and after 5 MeV, it becomes above the experimental data.

When we use g from Thomas-Fermi in one component of Ericson's formula, we observe this agreement, but when we use the same g in other PLD formulae such as two-component Ericson's formula, Williams, spin, and surface, we cannot notice this agreement. Other theoretical curves, resulting from substituting g from Thomas-Fermi in other PLD formulae such as two-component Ericson's formula, Williams's formula, spin formula, and surface formula, fall below the experimental curve. All theoretical curves start at 1 MeV and increase noticeably as the energy increases.

Acknowledgment

I would like to thank the Department of Physics, College of Sciences for Women, University of Baghdad for their support in writing this research.

Conflict of Interest

The authors declare that they have no conflicts of interest.

Funding

None.

References

1. Guttormsen, M.; Jurado, B.; Wilson, J.N.; Aiche, M.; Bernstein, L.A. Constant-Temperature Level Densities in the Quasi continuum of Th and U Isotopes. *Physical Review C—Nuclear Physics* **2013**, *88(2)*, 024307. https://doi.org/10.13251/DotB.2023.183.917
2. Pandit, D.; Bhattacharya, S.; Mondal, D.; Roy, P.; Banerjee, K.; Mukhopadhyay, S. Experimental Signature of Collective Enhancement in Nuclear Level Density. *Physical Review* C. **2018,** *97(4)*, 041301. https://doi.org/10.17751/DwNB.2023.183.933
3. Alwan, T.A.; Hameed, B.S. Study the Nuclear Structure of Some Even-Even Ca Isotopes Using the Microscopic Theory. *Baghdad Science Journal* **2023,** *20(1)*, 235-245.
4. Mohammad, J.F.; Salloum, A.D.; Al-Jabbar, H.A. Effects of the Changes in the Neutron Number of Isotonic Nuclei on the Tow-Component Partial Level Density Formula Corrected for Pairing in Pre-Equilibrium Reactions. *Iraqi Journal of Science* **2022,** *63(5)*, 1977-1981. https://doi.org/10.15251/DJNB.2023.183.927
5. Běták E.; Hodgson, P. Particle-Hole State Density in Pre-Equilibrium Nuclear Reactions. *University of Oxford, available from CERN Libraries, Geneva, report ref*. **1998,** *2*, 483-524. OUNP-98-02. https://doi.org/10.13351/Drt.2023.183.9017
6. Popa, G.; Baker, F. Systematics of Nuclear Level Densities. *Nuclear Theory*. **2014,** *33(14)*,187-192. https://doi.org/10.15251/DrsB.2023.133.347
7. Shafik, S.S.; Flaiyh, G.N.; Ali, A.M. Nuclear Level Density Parameter of 161−168Er and 204−210Bi Deforme Nuclei. *Al-Nahrain Journal of Science* **2014**, *17(3)*, 81-87.
8. Jasim, M.H.; The Effect of Deformation Parameter of Heavy Nuclei on Level Density Parameter. *Iraqi Journal of Physics* **2014,** *12(25)*, 38-43. https://doi.org/10.13451/DuyB.2023.183.12
9. Abdullah, A.M.; Salloum, A.D. A Comparison Between the Theoretical Cross Section Based on the Partial Level Density Formulae Calculated by the Exciton Model with the Experimental Data for Au Nucleus. *At energy*. **2020,** *78(198)*, 79-88. https://doi.org/10. 15251/DerB.2023.183.457
10. Karampagia, S.; Zelevinsky, V. Nuclear Shell Model and Level Density. *International Journal of Modern Physics E* **2020**, *29(6)*, 2030005. https://doi.org/10.15251/SERB.2023.543.917
11. Shil, R.; Banerjee, K.; Roy, P.; Sadhukhan, J.; Rana, T.K.; Mukherjee G. Isospin Dependence of Nuclear Level Density at A≈ 120 Mass Region. *Physics Letters B*. **2022**, *10*, 831:137145.
12. Astm, C. R23 Standard Test Methods for Determination of Water Absorption and Associated Properties by Vacuum Method for Pressed Ceramic Tiles and Glass Tiles and Boil Method for Extruded Ceramic Tiles and Non-tile Fired Ceramic Whiteware. *Appl. Phys.* **2018,** *21(2)*, 23-34.

13. Astm, C. Standard Test Methods for Apparent Porosity, Water Absorption, Apparent Specific Gravity, and Bulk Density of Burned Refractory Brick and Shapes by Boiling Water. *Appl. Phys*. **2022,** *11(12)*, 43-64.
14. Neamah, Z.J.; Mahdi, S.H.; Effect of zirconia addition on thermal and mechanical properties of poly-methyl methacrylate composites. *Digest Journal of Nanomaterials and Biostructures* **2023**, *18*, 927-932. https://doi.org/10. 15251/DJNB.2023.183.927
15. Lazaratou, C.V.; Vayenas, D.V.; Papoulis, D. The role of clays, clay minerals and clay-based materials for nitrate removal from water systems: *A review Applied Clay Science* **2020,** *185*, 105377. https://doi.org/10.1016/j.clay. 2019.105377
16. Ken, L. X-ray Diffraction, A program to analyze energy and angular dispersive, X-ray diffraction patterns. *Appl. Phys*. **1992,** *5(2)*, 45-56.
17. Astm, A. International Center for Diffraction Data, File™ & Related Products. *Jour. Phys.* **2009,** *2(11)*, 33-45.
18. Yasushi, S.; Norihiko, K. Quantitative Analysis of Tridymite And Cristobalite Crystallized In Rice Husk Ash By Heating. *Industrial Health* **2004**, *42*, 277–285
19. Laurence, N.W. Recommended abbreviations for the names of clay minerals and associated phases, *Clay Minerals* **2020**, *55*, 261–264. https://doi:10.1180/clm.2020.30
20. Lenz, S.; Birkenstock, J.; Fischer, L.A.; Schüller, W.; Schneider, H.; Fischer, R.X. Natural mullites: chemical composition, crystal structure, and optical properties, *Eur. J. Mineral* **2019**, *31*, 353–367, https://doi.org/10.1127/ejm/2019/0031-2812
21. Igami, Y.; Ohi, S.; Kogiso, T.; Furukawa, N.; Miyake, A. High-temperature structural change and microtexture formation of sillimanite and its phase relation with mullite. *American Mineralogist* **2019**, *104*, 1051-1061.https://doi.org/10.2138/am-2019-6732
22. Israa, M.R.; Yousif, I.M.; Takialdin, A.H.; Interactions Investigation of New Composite Material Formed from Bauxite and Melamine-Urea Formaldehyde Copolymer. *Ibn Al-Haitham Jour. for Pure & Appl. Sci*. **2016**, *29*(*1*), 181–192. https://doi.edu.iq/index.php/j/article/view/57
23. Mingye, W.L.; Ma, B.L.; Wenjian, Z.; Hao, Z.; Guangshun, W.; Yudong, H.; Guojun, S. One-step generation of silica particles onto graphene oxide sheets for superior mechanical properties of epoxy composite and scale application. *Composites Communications* **2020**, *22*, 1–7. https://doi.10.science /article/abs/pii/S2452213920302424.
24. Xiaomin, Y.; Bo, Z.; Xun, C.; Jianjun, L.; Kun, Q.; Junwei, Yu. Improved interfacial adhesion in carbon fiber/epoxy composites through a waterborne epoxy resin sizing agent. *Journal of Applied Polymer Science* **2017**, *134(17)*, 1–11, https://doi:10.1002/app.44757.10.1002.
25. Adil, I.K.; Dhefaf, H.B.; Zainab, S.A. The Effect Of Phoenix Dactylifera L. Pinnae Reinforcement On The Mechanical And Thermal Properties Of Polymer Composite. *Journal of the college of basic education* **2019**, *104(25*), 339–349. https://doi:index.php/cbej/article /view/4654.
26. Radhika, W.; Niharika, T.; Ashok, M.R. Mechanical and curing behavior of epoxy composites reinforced with polystyrene-graphene oxide (PS-GO) core-shell particles. *Composites Part C: Open Access* **2021**, *5*, November, 1–13, https://doi:10.1016/j.jcomc.2021.100128.
27. Zhaofu, W.; Rong, Qi.; Jin, W.; Shuhua, Q. Thermal conductivity improvement of epoxy composite filled with expanded graphite. *Ceramics International* **2015**, *41*, 13541–13546. https://doi:10. 1016/j.ceramint.2015.07.148.
28. Sravanthi, K.; Mahesh, V.; Rao, B.N. Influence of carbon Particle in Polymer matrix composite over mechanical Properties and tribology behavior. *Arch. Metall. Mater* **2019**, *66(4)*, 1171–1178. https://doi.bibliotekanauki.pl/articles/2049147.
29. Abdulhameed, R.A. Study on adhesion wear damage done on the hybrid composite Novolac under the experimental variables. *Energy Procedia* **2019**, *157(1)*, 644–654. https://doi.10. S1876610218311998.

30. Mustafa, B.H.; Salah, N.A.; Qabas, R. An Investigation of Tensile and Thermal Properties of Epoxy Polymer Modified by Activated Carbon Particle. IOP Conference Series: *Materials Science and Engineering* **2021**, 1094, *1*, 1–9, https://doi:10.1088/1757-899x/1094/1/012164.
31. Nuo, X.; Chunrui, L.; Ting, Z.; SiQiu, Y.; Liu, D.Z.; Dingshu, X.; Guocong, L. Enhanced mechanical properties of carbon fiber/epoxy composites via in situ coating-carbonization of micron-sized sucrose particles on the fiber surface. *Materials and Design* **2021**, *200*, 1–10, https://doi:10.1016 /j.matdes. 2021.109458.